Soft Matter

PAPER

View Article Online
View Journal | View Issue

Cite this: *Soft Matter*, 2024, **20**, 813

Characterization of drying-induced changes in moduli and internal stresses in a constrained gel using laser vibrometry†

Karthik Yerrapragada, Haocheng Yang, Wonhyeok Lee and Melih Eriten*

Received 4th October 2023,
Accepted 14th December 2023

DOI: 10.1039/d3sm01328f

rsc.li/soft-matter-journal

Hydrogels, water-saturated polymer networks find widespread use in soft robotics, biomedical, pharmaceutical and food industries. Both solid and water constituents of hydrogels are sensitive to external stimuli such as temperature, humidity, osmolarity, and light. For instance, common hydrogels swell or shrink in the presence of chemical potential gradient between the sample and surrounding environment. Corresponding changes in internal water content lead to significant changes in mechanical properties of hydrogels. Besides, internal stresses build up if the gel samples are constrained during swelling or dehydration. In the present research, we utilize modal analyses technique on drying hydrogels to identify dehydration-induced changes in elastic moduli and internal stresses. In particular, natural frequencies and damping ratios of the first two axisymmetric transverse vibration modes are measured on clamped gelatin disks using non-contact laser vibrometry at various water loss states. Experimental modal frequencies are then compared to the predictions of a pre-stressed thick plate model. The evolutions of elastic moduli and internal stresses for water losses up to 80% are identified. The broadband loss capacity of gelatin is also determined from the measured modal damping ratios. Highly transient mechanical response observed on the gelatin disks further demonstrates the need for non-contact and rapid mechanical characterization of hydrogels. As illustrated in this work, vibration and wave-based techniques are promising candidates to fulfill that need.

1 Introduction

Soft materials often undergo visible elastic deformation upon application of small forces.[1] Hydrophilic polymer networks swollen by water are an important class of soft materials in medicine, food industry, structural and robotics.[2–9] Multiphasic nature of hydrogels leads to considerable variations in mechanical properties and internal stresses with changing operating conditions such as temperature, humidity and osmolarity.[10] Proper characterization of evolution of material properties[11] and internal stresses due to constrained boundaries[12] are critical in reliability and safety of hydrogels in load-bearing applications as listed in ref. 13. For instance, the performance of injectable hydrogels as vocal cord replacements would depend heavily on changing levels of humidity, temperature, pH in human body.[14] In addition, hydrogels are being used in high-strength and load-bearing applications.[13]

Mechanical properties of hydrogels are characterized conventionally by rheometry, uniaxial tension/compression and indentation.[15–19] Those tests are conducted on specialized commercial testers with specially-prepared samples and fixtures. The samples are either partially or fully destroyed during the tests. Therefore, high throughput measurements with conventional techniques are resource-intensive and time-consuming, and thus not suitable for *in operando* characterization. Vibration and wave-based characterization offers a viable alternative for soft materials.[20–26] For instance, laser vibrometry[21] is shown to characterize dynamic and viscoelastic properties of multiphasic biological tissues such as cartilage considerably faster than conventional techniques.[21] Studies utilized vibration techniques to understand parametric resonances in soft materials and water droplets;[27] develop variable stiffness artificial muscles for vibration absorption;[28] and achieve broadband vibration attenuation using soft materials.[29] Vibration-based monitoring of mechanical properties of various plants also delivers important information on plant genetics and phenotyping.[30,31]

Recent applications of vibration-based techniques on hydrogels are promising for accurate, non-destructive and quick mechanical characterization.[8,10,11,32,33] In particular, Schwarz *et al.* measured the axisymmetric vibration modes of circular gelatine plates. The work identifies the elastic moduli from modal frequencies and compares them with the values obtained *via* atomic force microscopy and uniaxial compression.[11] Similarly, Kim *et al.* utilizes video-based vibrometry to obtain natural frequencies and moduli of hydrogel structures.[8] Wang *et al.*[10]

Department of Mechanical Engineering, University of Wisconsin-Madison, Madison, 53706, WI, USA. E-mail: eriten@wisc.edu

† Electronic supplementary information (ESI) available. See DOI: https://doi.org/10.1039/d3sm01328f

monitor modal damping ratios of beams made of polyacrylamide hydrogels. They report that hydrogels have significantly lower damping than PDMS, making them a suitable material system for vibration and wave-propagation applications. Another recent study by Guisquet and Amabili successfully extracts viscoelastic properties of hydrogel samples from vibrations during highly transient sol–gel transition.[33]

Dynamic mechanical analysis and rheometry deliver the storage and loss moduli of materials over a range of loading frequencies. Gels with low stiffness (high water content) and high adhesion can result in sample sticking during DMA techniques as described inref. 33. Our group also observed high adhesion when testing oil-imbibed open cell foams with indentation-based DMA.[23] One needs to suppress adhesion *via* surface treatment and/or lubrication in those techniques to reuse the samples. However, that would also trigger nonlinear interfacial mechanics such as slip and make the identification harder. Shear wave and optical coherence elastography provide mechanical characterization by imaging waves and static/dynamic strains induced by often contact-based actuators. The moduli of the material actuated are then identified from the shear wave speeds and strain magnitudes with an assumed constitutive behavior. Internal stresses, dispersion and impedance contrasts could lead to significant scatter and losses in wave and strain amplitudes, and could hinder accurate identification of moduli in complex soft materials.[34–38] In simpler cases, especially when the gels are homogeneous and stress-free (in as-cured state), those methods can be used to identify material properties as well as vibration-based techniques.

Inspired by the recent successes of vibration-based characterization, we conduct modal analyses, and investigate drying-induced changes in elastic moduli and internal stresses in constrained gelatin disks. Note that hydrogels can swell or dehydrate depending on the chemical potential gradient between the sample and surrounding medium, and changing water amount inside the sample can lead to orders of magnitude changes in mechanical properties.[4,39–42] Li *et al.*,[40] for instance, provide a scaling relation that explains swelling and deswelling-induced variations observed in elastic moduli and fracture energies of hydrogels. Besides the changes in mechanical properties, de/swelling under constrained configurations would result in built-up of internal stresses. In general, vibration-based techniques require the knowledge of internal stresses to account for their influence on measured wave speeds and identify elastic properties accurately. Extensive acoustoelasticity literature on engineering structures such as beams, frames, trusses, plates and shells exemplify how internal stresses alter modal frequencies.[43–48] Those structures are made of engineering materials mechanical properties of which can change significantly only under extreme temperatures and pressures.

The above-mentioned studies on vibration-based characterization neglect the changes in material properties as their samples and experimental protocols prevent excessive water gain/loss. It is known that hydrogels with low polymer fractions can lose 80% of their original water content when left or tested under ambient conditions for extended duration, as will be demonstrated in this work. That huge change, under constrained geometries will lead to simultaneous alterations of elastic moduli and internal stresses. In this work, we conduct laser vibrometry on constrained gelatin disks and characterize drying-induced evolution of material properties and internal stresses. To the best of the authors knowledge, such a characterization over a broad range of water losses is missing in the literature. In addition, we clearly demonstrate that internal stresses should be accounted for in vibration-based mechanical characterization of constrained soft multiphasic materials. If not, unreasonably high (small) moduli can be identified under tensile (compressive) internal stresses. Specific to the dehydrated gel disks that we tested here, the mean moduli identified without internal stresses can reach five times the mean moduli identified with internal stresses. Such an error is undesirably large for mechanical characterization.

In Section 2, we provide details of the sample preparation, vibration tests, gel dehydration and brief description of the modal frequencies obtained from the pre-stressed thick plate model (more details and derivation can be found in Section S1 of the ESI†). In Section 3, we report the drying-induced changes in modal frequencies and damping ratios, and identify the elastic moduli and in-plane stresses as a function of water loss during dehydration.

2 Methods and analysis

2.1 Sample preparation

Disk samples are prepared by mixing gelatin powder (7201A Gelatin, Type 1, Neogen Corp.) into water with 10% (w/v) concentration. The mixture is then heated to 50 °C and stirred with a magnetic stir bar (Vevor) at 150 rpm until homogeneous solution is achieved. Food coloring agent (Wilton Brands LLC) is added to the solution with 0.1% (v/v) concentration to obtain dark green solution for stronger laser reflection and enhanced signal-to-noise ratio in vibration tests. The solution is then degassed using a vacuum pump (3.6 CFM, 1/4 HP, Vevor) and chamber (1.5 gal, Vevor), and poured into several 3d printed fixtures to form the hydrogel disks shown in Fig. 1A. The radius of each disk as set by the designed fixture geometry is 15 mm. Volume of the solution that is poured is controlled to obtain a target average thickness of 4 mm. Smaller thicknesses lead to geometric changes due to self-weight during transportation and curing of gels. In addition, after the curing process is complete, thicker samples which have higher bending rigidity can overcome any gravitational effects. A small amount of super glue (Gorilla Glue Inc.) is applied to the fixtures to ensure sticking boundary with the poured gel and simulate clamped boundary condition. After the gel disk samples in solution state are created to the desired thickness, they are left to rest for 5 minutes at room temperature to allow curing sufficient for transportation. The samples are then wrapped by thin PVC films to prevent dehydration and refrigerated for 1 hour at 4 °C for rapid curing. Before vibration testing, the cured disk

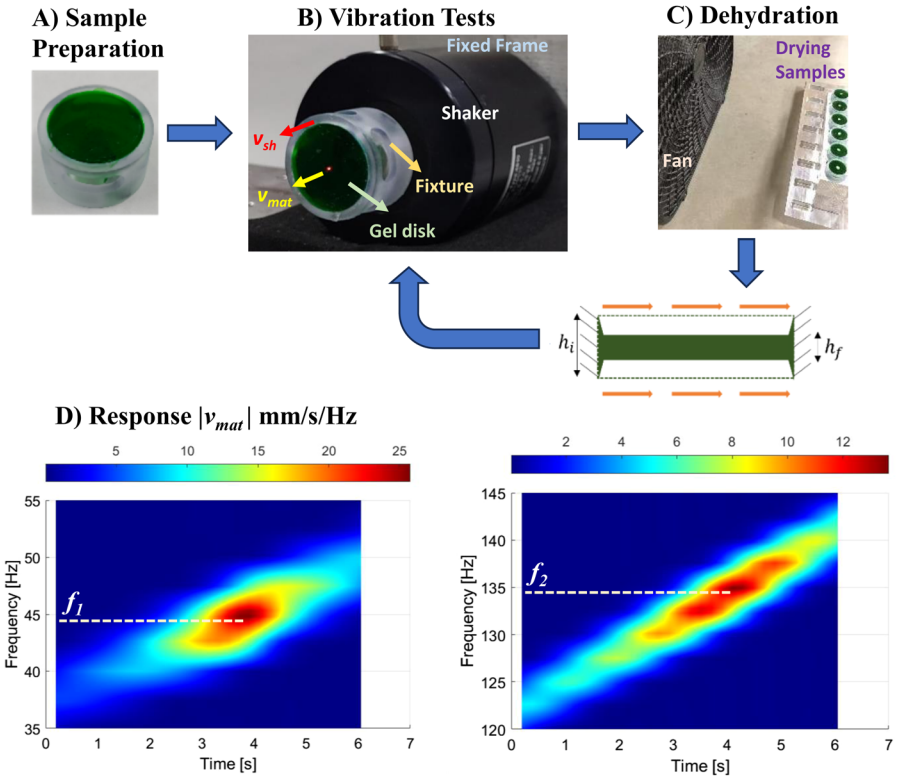

Fig. 1 Experimental details: (A) gelatin preparation and curing to a fixture; (B) components in vibration testing; (C) dehydration process, and (D) representative time-frequency-amplitude plots of the material response $|v_{mat}|$ around mode 1 and mode 2 as processed from frequency sweep data.

samples are removed from the refrigerator and left to equilibrate at room temperature for 5 minutes.

2.2 Vibration tests and dehydration

Next, the fixtures with the disk samples are connected to a shaker (Type 4810, Bruel&Kjaer) *via* 10–32 internal threads at the bottom (see Fig. 1B). The 3D printed fixtures can be assumed rigid within the frequency range of interest (<500 Hz) as the lowest fixture mode is found to be greater than 1 kHz. Initially, each fixture is subjected to a sine-sweep (0 to 1 kHz within 10 s) at small amplitudes, 20 μm peak to peak shaker displacement and 300 μm peak to peak material displacement at resonance. The velocity of the material point in the middle of the attached gel disk v_{mat} is measured by a scanning laser vibrometer (PSV-400, Polytec, Inc.) to coarsely identify the frequencies of the axisymmetric modes. In this study, the focus will be on the first two axisymmetric modes. After coarse identification of the modal frequencies for a given sample, we perform fine sine sweeps (sweep rates range between 2.5–4 Hz s^{-1}) around the resonances to accurately obtain the modal frequencies (f_1 and f_2) and damping ratios (ζ_1 and ζ_2) of those two modes. To verify the axisymmetry, we also conduct scanning vibrometry at resonances and obtain the mode shapes of those two modes on an independent sample in the wet and dry (water loss of 80 wt%) states. The vibration of the material point is sampled at 2.56 kHz in those fine sweeps. Representative time–frequency plots of the instantaneous amplitudes (spectrogram, mm s^{-1} Hz^{-1}) of the material response, $|v_{mat}|$ are shown in Fig. 1D for the two modes, where the peak responses are used to identify the modal frequencies f_1 and f_2, and half-power method is used to identify the corresponding damping ratios ζ_1 and ζ_2.

The same vibration testing is performed for all six samples under ambient conditions, 25 °C and 30–40% RH. Total time to complete the vibration testing of all samples is 30 min (5 min per sample) while they are in the wet state. The weight of the samples is monitored before and after the vibration tests and the water loss is determined as the weight percentage (wt%).[49] After the first round of vibration testing, the average water loss is measured as ~4 wt%. Before the subsequent rounds, the samples undergo accelerated dehydration *via* air flow provided by a fan (see Fig. 1C). Samples are weighed every 5 min to achieve target water losses around 15, 30, 45, 60 and 75–80 wt%. At each water loss state, another round of vibration testing and modal analysis is completed on each sample. Note that the dehydration rates under ambient conditions (about 0.15% per min) are an order of magnitude lower than under air drying (about 1.6% per min). Therefore, additional drying during vibration testing has a minor influence to the measured modal parameters. Those vibration tests on six samples at six different water loss including the as-cured (wet) states, will help us investigate the drying-induced changes in modal parameters.

2.3 Pre-stressed thick plate model

The theoretical model based on Mindlin plate theory to describe the transverse linear vibrations of the gelatin disk

with initial stress is shown in eqn (1) and (2) in a non-dimensional form (ref. 46).

$$\frac{\kappa}{2(1+\nu)}\left(\frac{\partial^2 W}{\partial \xi^2}+\frac{1}{\xi}\frac{\partial W}{\partial \xi}+\frac{\partial \psi}{\partial \xi}+\frac{\psi}{\xi}\right)+\beta\left(\frac{\partial^2 W}{\partial \xi^2}+\frac{1}{\xi}\frac{\partial W}{\partial \xi}\right)=W'' \tag{1}$$

$$\left(\frac{1}{1-\nu^2}+\beta\right)\left(\frac{\partial^2 \psi}{\partial \xi^2}+\frac{1}{\xi}\frac{\partial \psi}{\partial \xi}-\frac{\psi}{\xi^2}\right)-\frac{6\kappa\alpha^2}{1+\nu}\left(\frac{\partial W}{\partial \xi}+\psi\right)=\psi'' \tag{2}$$

where $W(\xi,\tau)$ and $\psi(\xi,\tau)$ are the transverse displacement and the rotation of the cross section with respect to the undeformed configuration and they depend on the radial position only considering only axisymmetric vibration. Detailed derivation of eqn (1) and (2) from dimensional form can be found in Section S1 of the ESI.† The disk is subjected to uniformly distributed initial in-plane tension or compression. The in-plane force is assumed to yield uniformly distributed initial stress σ_0 along the radial and the circumferential direction only. α and β are defined as

$$\alpha=\frac{R}{h_f},\quad \beta=\frac{\sigma_0}{E} \tag{3}$$

The peak to peak vibration amplitudes at resonance are smaller than the thickness of the sample (around ratio of 0.1). Thus, linear perturbation assumption holds true for the vibration analysis. Galerkin's method is used to obtain the non-dimensional modal frequency defined as

$$\lambda_n=R\omega_n\sqrt{\frac{\rho}{E}} \tag{4}$$

and the solution is influenced by α, β, Poissons ratio ν and shear correction factor κ. From eqn (4), one can see that the ratio between λ_n of the second and the first mode is the same as the ratio between ω_n of those modes at a given water loss state.

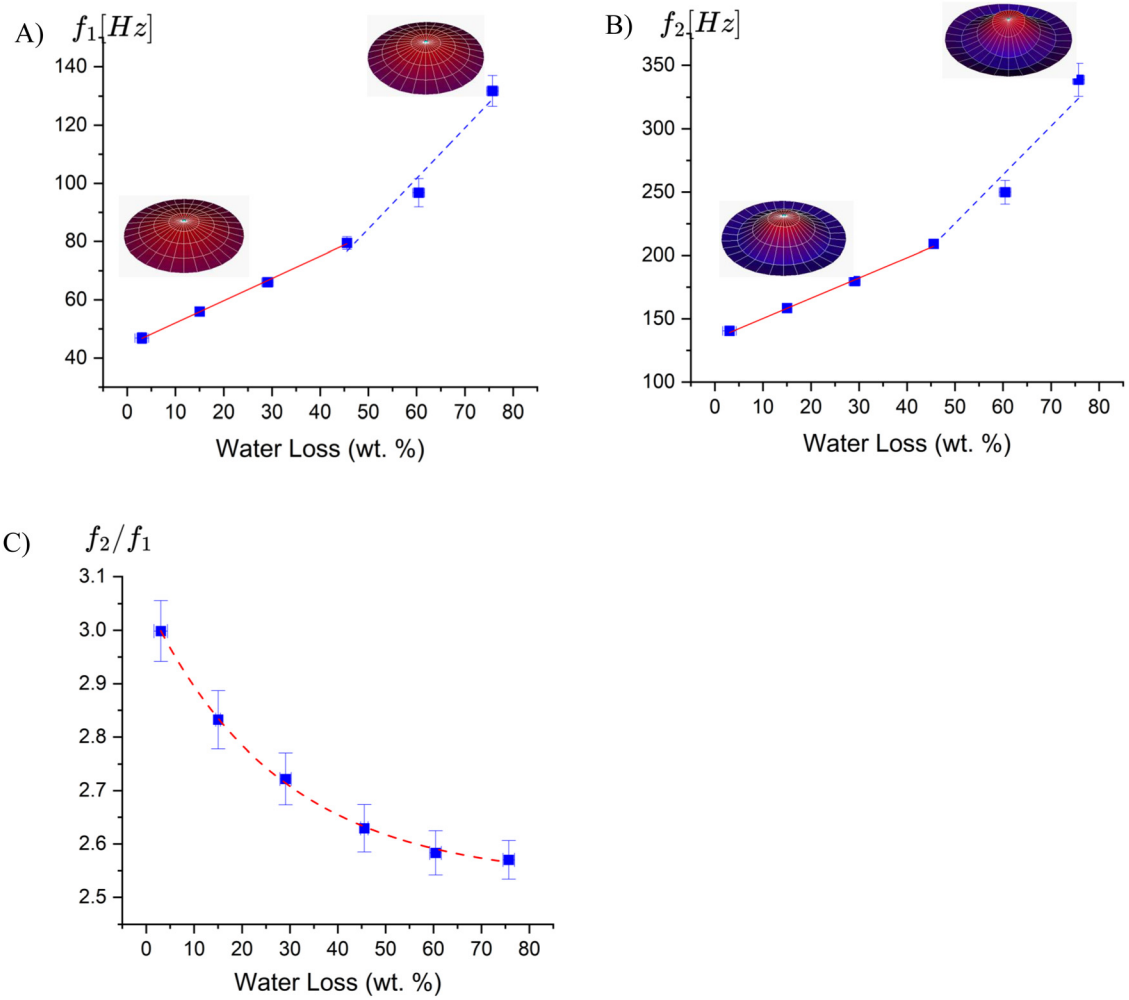

Fig. 2 Evolution of modal frequencies with water loss: (A) first mode frequency f_1; (B) second mode frequency f_2, and (C) frequency ratio f_2/f_1. The dashed curves denote the regression analysis.

The full process of obtaining λ_n and mode shapes from eqn (1) and (2) is also described in Section S1 of the ESI.†

3 Results and discussion

3.1 Modal frequencies

Fig. 2A and B show the drying-induced evolution of the first and second modal frequencies, respectively. The mean and standard deviation of frequencies are presented in Fig. 2. The samples show similar water loss levels as evident with low error levels along x-axis. At all water losses, samples possess reasonably close modal frequencies, which suggests consistency in sample preparation, initial geometries, and dehydration process. Both mode shapes at extreme water loss states on an independent sample confirm axisymmetric profiles (inset isometric view plots in Fig. 2A and B). In addition, the theoretical mode shapes are compared with experiments in Fig. S1 and S2 of Section S2 of the ESI† for extreme water loss states. For all samples, both modal frequencies increase with dehydration; nearly 3-fold for the first mode and 2.5-fold for the second. There are three factors to consider in explaining that increase. First, as the samples lose water, their volume shrinks. This leads to thickness reduction since the disks are glued to the fixture to ensure clamped boundary conditions; radii of disks are fixed at 15 mm. Reduction in thickness, however, would lead to reduction in bending rigidity and thus modal frequencies. Secondly, water loss in a sample inherently means increase in polymer fraction, and gels with higher polymer fractions are stiffer; *i.e.*, have higher elastic modulus.[40,50,51] The increase in modulus definitely helps explain the increases in modal frequencies. Note that the elastic modulus and density of a sample define the wave speed, and the thickness is the only geometric factor aside from the disk radius influencing the modal frequencies. At a given water loss state, all of those quantities are expected to be close if not near identical. Therefore, the ratio of modal frequencies would cancel out both the wave speed and geometric factors and deliver a constant value, frequency ratio, f_2/f_1. For instance, frequency ratio for the axisymmetric modes of a thin circular clamped plate (Kirchoff plate) is around 3.9 whereas for a thick plate (Mindlin plate) as our samples, it is around 3.[52,53] Fig. 2C shows the measured evolution of frequency ratios with dehydration. Note that the frequency ratios cluster around 3 for as-cured samples ($\sim$0 wt% water loss), and this is in agreement with the thick plate theory. However, as the water loss increases, the frequency ratios decrease and nearly saturate between 2.5 and 2.6 for the samples at extreme 70–80 wt% water loss states. Considering that plate theories suggest drying-induced thickness reduction would further increase the frequency ratio, another dominant factor must be behind the significant increase in modal frequencies. This leads us to study the third possible factor: in-plane stresses that build up due to constrained dehydration. As well-known in above-mentioned plate theories, in-plane stresses would decrease the frequency ratios. In fact, when in-plane stress dominates the bending rigidity, membrane approximation would be applicable for vibration modes, where wave speed is largely determined by the in-plane stress. In this asymptotic case, more dehydration would lead to increase in in-plane stress and thus in wave speed and modal frequencies. Besides, the frequency ratios for the lowest two axisymmetric membrane modes is approximately 2.3, which is quite close to the lowest frequency ratio shown in Fig. 2C.

Regression analysis is performed on the data using Origin 2023b (OriginLab Co., US) to determine the trends. The natural frequencies of the first two modes show strong linear trend, $f_i = A_i + B_i x$ where x is the water loss in wt%. At low water loss (up to 45%) the slopes B_i's are (0.76, 1.59) with R^2 = (0.99, 0.99). At higher water loss from 45% up to 75%, the frequencies increase at higher slopes for the two modes (1.73, 3.84) with R^2 = (0.96, 0.96). Along with the material modulus, the internal stress effect also increases. The evolution of frequency ratio are fit to a decaying exponential function of water loss $f_2/f_1 = 2.53 + 0.52e^{-0.036x}$ with R^2 = 0.99. This fit quantifies asymptotics of physical response: at zero water loss the fit yields a frequency ratio of 3.04, which is close to the predictions of thick plate theory. At high water loss asymptotic, the fit predicts 2.53, a frequency ratio close to membrane modes.

In summary, out of the three changes induced by dehydration, increase in elastic modulus and in-plane stresses promote increasing modal frequencies while reduction in thickness has an opposite effect. Next, we will analyze the experimental modal frequencies further against predictions of the pre-stressed thick disk model.

3.2 In-plane stress and elastic moduli

Predictions of pre-stressed thick plate theory can provide reference for how radial in-plane stress and elastic modulus of the gelatin disks evolve with drying. However, before we can estimate modal frequencies of a pre-stressed thick plate, we need the thickness of the disks, h_f at each water loss state. As a first order approximation, we first convert the water losses measured as wt% to volumetric changes and assume that the whole disk will endure similar volumetric change. We set the density of the gels to ρ = 1120 kg m^{-3} while converting weights to volumes. The gelatin density values set is similar to the values obtained in literature.[11,54] Since the radius of the disk is fixed, then that change will be fully reflected on the thickness; *i.e.*, thickness will reduce the same amount as water loss. This approximation assumes uniform thickness reduction and omits the out-of-plane strains due to radial in-plane stresses (bi-axial loading in radial and circumferential directions). Upon visual inspection of the dehydrated samples, we confirm nearly uniform thickness reduction except for the boundary of the disks where the gels are glued to the fixtures. Modal parameters would not be sensitive to the variable thickness around the boundaries for a clamped configuration. Omission of out-of-plane strains is justifiable only for small pre-strains. Since in-plane stresses and strains were initially unknown to us, we measured drying-induced thickness reduction on independent samples and confirmed that near identical reduction in thickness and water amount (see Fig. S3 in Section S3 of the ESI†).

For large strains under volumetric changes, nonlinear stress-diffusion problem and poroelasticity needs to be considered in gels, *e.g.*, ref. 55–60.

After relating the thickness of the disks, h_f to the degree of water loss, we can determine the frequency ratios from the thick plate theory as a function of in-plane stress normalized to elastic modulus $\beta = \sigma_0/E$, which can also be interpreted as a measure of pre-strain. From the equations of motion, one can obtain another non-dimensional parameter influential in modal frequencies, radius-to-thickness ratio of the disks, R/h_f. Since we can estimate that parameter from the experimentally inferred thickness, β serves as the only free parameter that control the frequency ratio. Assuming homogeneous, isotropic, linear elastic material response and uniform radial in-plane stress distribution, we estimate the β values for all samples at different water loss states. The mean and standard deviation frequencies of the six samples for the identified internal stress and Young's moduli are shown in Fig. 3A and B. Fig. 3A shows the evolution of the estimated β values with dehydration. At as-cured (wet) state, β values cluster around 0, meaning that the in-plane stresses in the gelatin disks are negligibly small, and reach up to 0.12 at 60 wt% water loss state. This range of average radial in-plane strains verify small strain linear elastic response for gelatin as reported elsewhere.[18,19] For a couple of samples, negative values of β; *i.e.*, compression is needed in the theory to match the experimental frequency ratios at the wet state. This is primarily due to variations in the initial thickness h_i, which we control solely with solution volume poured into disk shape during sample preparation. Note that $\beta = \sigma_0/E$ increases with water losses up to 60 wt% water loss state, and then reduces slightly upon further drying. One would expect nominal in-plane stresses σ_0 to be a non-decreasing function of water loss. Hence, we anticipate that dehydration beyond 60 wt% induces more rapid increase to elastic modulus E than it does to in-plane stress σ_0, and thus normalized in-plane stresses quantified by $\beta = \sigma_0/E$ decreases.

To further check that, we estimate the elastic moduli from the first modal frequencies measured at each water loss state, and show it in Fig. 3B. Note that estimations from the second modal frequency would deliver identical results as the normalized parameter $\beta = \sigma_0/E$ is estimated from the measured frequency ratios. The elastic moduli E estimated for all samples increases from 40 kPa at the wet state to 130 kPa at the 60 wt% water loss state. Further drying induces a sharp increase in moduli, around 300 kPa at 75 wt% and 550 kPa at close to 80 wt% water loss states. This rapid stiffening of the gels explains the slight reduction of the normalized in-plane stresses $\beta = \sigma_0/E$ (Fig. 3A). The range of moduli estimated from the measured modal frequencies is consistent with the reported values for gelatin and various hydrogels.[10,11,18,19,33,51] Besides, de Gennes proposed that elastic modulus for swollen gels should scale with a power of 2.25 of concentration.[50] Moduli obtained from uniaxial compression of gelatin suggest concentration-dependent increase but with lesser scaling

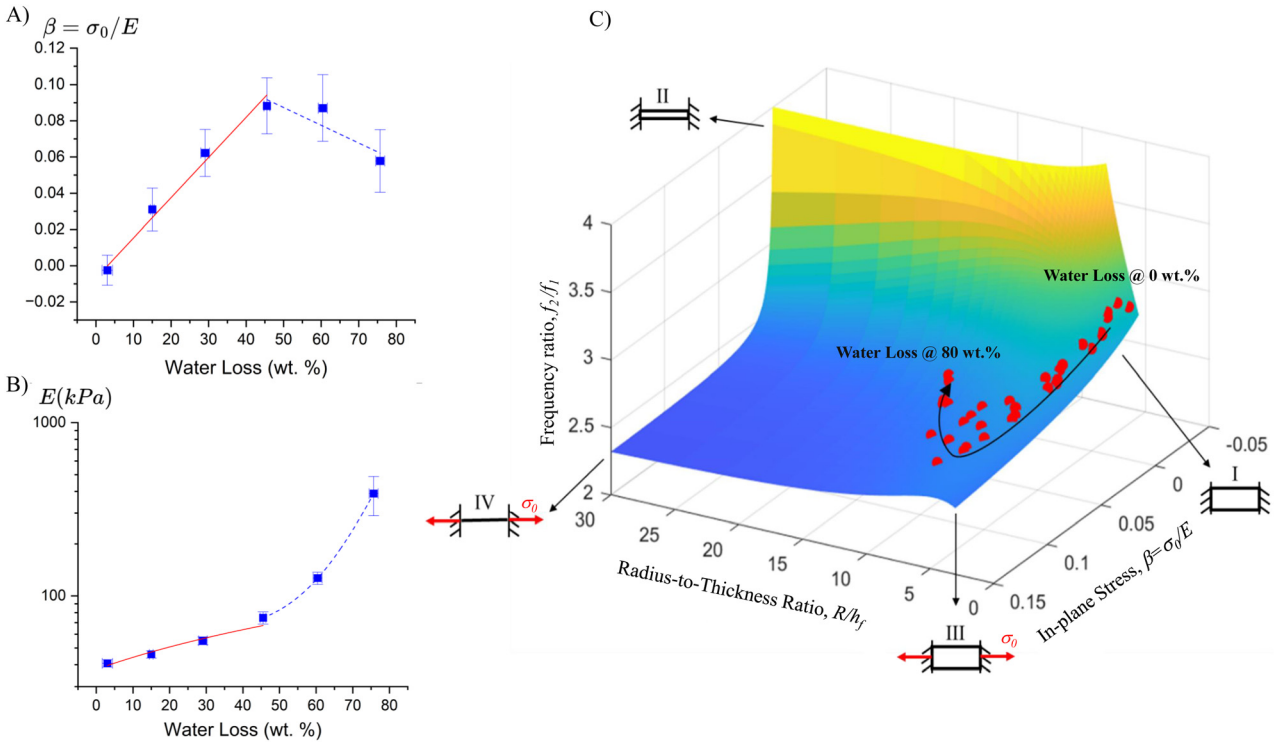

Fig. 3 (A) Evolution of normalized in-plane stress $\beta = \sigma_0/E$ with water loss; (B) evolution of estimated elastic modulus E with water loss, and (C) frequency ratio as a function of normalized in-plane stress and radius-to-thickness ratio. Markers in (C) correspond to the experimental data. Inset sketches in (C) illustrate four extreme conditions for the disks. Arrow in (C) indicates increasing water loss. The dashed curves denote the regression analysis.

powers than de Gennes' argument; *e.g.*, scaling powers ranging from 1.5 to 2 in ref. 61,62. Roughly, 80 wt% water loss state corresponds to 3.5-fold increase in concentration of the gelatin in our tests; *i.e.*, from 10 at the wet state to about 35% (w/v) at the extremely dry case. De Gennes' scaling law then predicts a 17-fold increase in the moduli. Recently, a different exponential scaling law is proposed by Xu *et al.* to explain dehydration-induced stiffening in polyacrylamide hydrogels.[51] Moduli reported in that work increase 9-fold with about 60 wt% water loss. Therefore, 14-fold increase we report in Fig. 3B is consistent with scaling laws and previous observations of concentration-dependent moduli. For internal stress parameter predictions, Fig. 3A, we can obtain linear trends for both low and high-water loss levels with slopes $(0.002, -9.8 \times 10^{-4})$ and $R^2 = (0.98, 0.80)$. The evolution of Young's modulus can be fit using a linear function up to 45% water loss levels with a slope 3.84 and $R^2 = 0.85$. Beyond 45% water loss, an exponential function $e^{0.1x}$ with $R^2 = 0.99$ is fit to capture the rapid and nonlinear growth in moduli.

To summarize the evolution of thickness and in-plane stresses of the tested gelatin disks, and corresponding frequency ratios, we project the experimental estimations on to the predictions of the pre-stressed thick plate theory in Fig. 3C. Note that the frequency ratio is a surface that can be fully parametrized by radius-to-thickness ratio R/h_f and normalized in-plane stress $\beta = \sigma_0/E$. Besides, for a set R/h_f value, frequency ratio is a one-to-one function of β. Therefore, once complemented with one of the modal frequency expression, measured frequency ratios can deliver in-plane stress σ_0 and modulus E uniquely for drying hydrogels. This paves the way for non-invasive, quick and *in operando* mechanical characterization for soft swollen materials. On the continuous frequency ratio curve predicted by the theory, we sketched side views of disks at four cases corresponding to extreme values of parameters R/h_f and β. Case I is the limiting case when both parameters are small; physically corresponding to a thick stress-free plate. As discussed above, the frequency ratio for that case is close to 3 as predicted by the Mindlin plate theory.[53] Case II corresponds to stress-free thin plate asymptote. Case III and IV are stressed versions of the thick and thin plates, respectively. Note that experimental data projected on the theoretical surface reveal that tested gelatin disks obey stress-free thick plate theory initially (Case I), and then evolved quickly towards stressed thick plate (Case III) and then take a turn towards stress-free thin plate (Case II) direction with increasing water loss. This evolution clearly demonstrates the major challenge of mechanical testing and characterization of soft multiphasic materials in uncontrolled operating conditions. The asymptotic cases providing simple estimations rarely represent the physical state of the gels being tested. Because we measure the water loss and infer major geometric changes, we could identify mechanical properties such as in-plane stresses and moduli from linear modal frequencies. In unconstrained settings, acoustoelasticity would promise similar identification.[63] On constrained systems without geometry information, one can utilize nonlinear vibrations in identification as an analog to large acoustoelastic effects[64] used in inverse problems. Also, in a hypothetical setting, one can neglect internal stress built-up and utilize only first modal frequency to estimate the moduli of the disks as done elsewhere.[11,34,65] The mean moduli identified by that method can reach to 2 MPa, five times the mean moduli that we identified (see Fig. S4 in ESI†). Such high moduli were not observed in the literature: moduli reported for bovine gelatin were lower than 180 kPa even at very high concentration values[66] and below 700 kPa for polyacrylamide hydrogels at 80% dehydration levels.[40,51] Besides, such identification would fail to predict higher modal frequencies as the frequency ratio remains unaltered without internal stress. Such an error is unacceptable for mechanical characterization. We also perform indentation-based characterization to cylindrical gel samples prepared identically as in gel disks. We obtain mean moduli around 33 kPa from five different indents. Those values are very close to $\sim$40 kPa obtained from vibration-based characterization shown in Fig. 3B (see Section S5 of the ESI† for details).

3.3 Modal damping ratios

In this work, we utilize frequency sweep tests to identify modal parameters. Alternatively, transient excitation could be used. In either case, amplitude and duration of vibrations are primarily controlled by damping of the hydrogels. The effect of water loss on damping ratios ζ_1 and ζ_2 is shown in Fig. 4A and B. For all cases, the damping ratios range from 2.7 to 5.7%. This range is consistent with reported values in ref. 10, 3 to 5.5% for polyacrylamide hydrogels. Damping ratios reported for poloxomer hydrogels are also close to our measurements; 1–2% in the fully-cured state.[33] In any case, those damping ratios deliver a minimum of 10-fold dynamic magnification around resonances and thus promise clear identification of modal frequencies even under small excitation. For the first mode, the damping ratio reaches a peak when the water loss is around 30 wt% and decreases with further drying. The damping ratio of the second mode exhibits a monotonically increasing trend with drying. This difference in damping ratio evolution leads to an interesting consequence for decay rates of individual modes throughout transient response. Next, we assume a linear viscoelastic response and convert the measured modal damping ratios to the loss tangent $\tan(\delta) \approx 2\zeta$ and map it against measured modal frequencies in Fig. 4C. Since the modal frequencies range from 40 to 350 Hz (Fig. 2A and B) during the dehydration process, this map provides a quick and broadband characterization of overall loss capacity of gelatin. The estimated loss tangent values vary from 6 to 10%, and that range is consistent with the ranges reported for other multiphasic soft materials such as gelatin from bovine skin;[66] polyacrylamide hydrogels,[10] and cartilaginous tissues extracted from condyle, patella, and meniscus regions of bovine knee joints.[21] Note that damping can be introduced by a complex modulus in the physical equations of motion (eqn (1) and (2)) or modal viscous damping added to the ODEs obtained after Galerkins projection. Damping parameters in either case would be fitted to the measured modal damping ratios. Since the loss tangent values quantifying the ratio of loss to storage moduli reside below 0.1 for all dehydration states, linear elastic

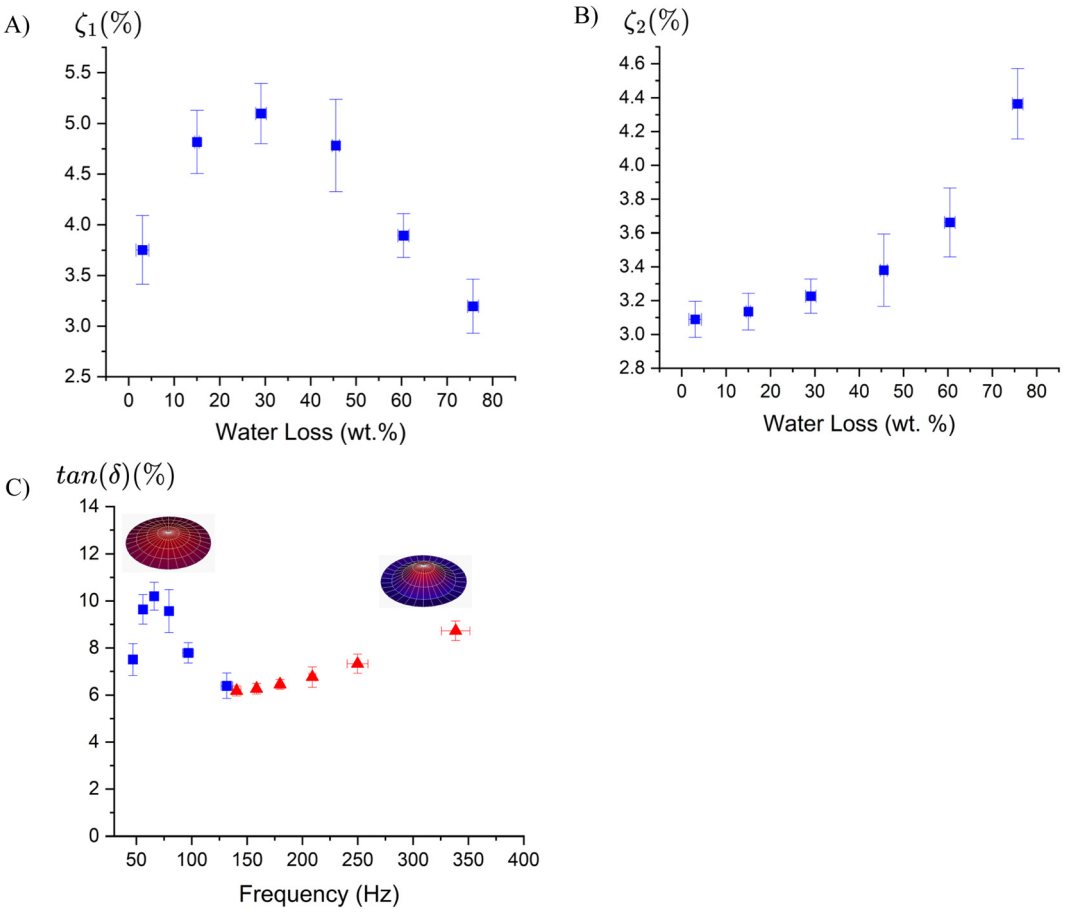

Fig. 4 Evolution of damping ratios with water loss: (A) ζ_1; (B) ζ_2; (C) loss tangent *vs.* frequency.

formulation we adopted in this paper would lead to less than 10% error in moduli estimation when compared to a viscoelastic formulation.

It is well-known that the dissipation in hydrogels can be due to poroelastic effects and viscous damping from the polymer chain network as observed by ref. 10. Considering that the diffusivity of gelatin is on the order of 10^{-10} m^2 s^{-1} and the smallest thickness that we measure at dry state is around 1.5 mm, we can obtain poroelastic time constant on the order of 10^4 s. The vibration frequencies that we measured are in the range of 40 to 350 Hz. Hence, poroelastic dissipation in a vibration cycle is expected to be negligible during vibration tests. The remaining source of damping is viscoelasticity, attributed to the load-induced reconfiguration of polymer network. The water content in the gel will influence the load-sharing between the polymer network and water, but diffusion-related losses will be very small compared to solid network reconfiguration and thus viscoelastic losses. Therefore, damping capacity shown in Fig. 4C report mostly viscoelastic dissipation stemming from solid network. One can envision that modal frequencies can coincide with poroelastic time constant for small samples at very slow loading rates; *e.g.*, very thin gels. Then, poroelastic dissipation would be as influential as viscoelasticity, and thus damping capacity would depend largely on modal frequencies and water amount – asymptotically reaching similar values as 75% dry cases.

Another interesting observation is about the decay rates that can be quantified by $2\pi\zeta_i f_i$. Commonly, decay rates of higher vibration modes are much larger than lower modes, and thus lower modes dominate the later stages of transient responses in structural materials. This separation in decay rates facilitates reliable mode decomposition, model order reduction and control for dynamic systems. However, for the gelatin disks at around 30 wt% water loss state, decay rates of the axisymmetric modes are close to each other; 24.19 and 35.06 rad s^{-1} for the first and second mode, respectively. Therefore, transient responses of gels at those water loss states would contain contributions from both modes at detectable levels of vibrations, adding another complication to transient-vibration-based identification of those materials, especially in nonlinear regimes.

4 Conclusion

In this article, we conducted modal analyses on drying gelatin disks and identified drying-induced changes in elastic moduli and internal stresses. In particular, we measured the forced response of the clamped gelatin disks subjected to frequency sweep excitations in the transverse direction and captured the

frequencies and damping ratios of the first two axisymmetric bending modes. We then dehydrated the samples and repeated the modal analyses at six different water loss states (0 to 80% water loss by weight). We observed that the modal frequencies increased nearly 3-fold for the first and 2.5-fold for the second mode. Measured damping ratios reached a peak around 30% water loss for the first mode and exhibited a monotonic increasing trend for the second mode. We then compared the experimental modal frequencies to the predictions of a pre-stressed thick plate model, and identified the elastic moduli and internal stresses as a function of water loss. Based on the identification process, the elastic moduli increased an order of magnitude while internal stresses reached up to 10% of elastic moduli with dehydration. At low water losses, the bending rigidity controlled the transverse vibrations, whereas at high water losses, the increase in internal stresses dominated the increase in bending rigidity and thus, the gelatin disks vibrated akin to pre-tensioned membranes. Without internal stress formulation, one can not explain the drying-induced changes in the frequency ratio, and elastic moduli estimations would be unrealistically high. Finally, we converted the measured modal damping ratios to the loss tangent, which demonstrated a quick and broadband (40–350 Hz) characterization of the loss capacity of gelatin. Highly transient mechanical response that we observed on the gelatin disks called for a non-contact and rapid mechanical characterization technique, and the vibration-based methodology that we outlined in this work clearly fulfilled that need.

Immediate applications of that methodology can be found in soft robotics, and agri-food, biomedical and pharmaceutical industries. For instance, hygroscopic actuators used in soft robotics experience significant dehydration-induced stiffening that influence their actuation energy and strain capacities.[67] Water-retaining hydrogel beads are utilized in sustainable agriculture to alleviate irrigation needs. Those beads swell and shrink while constrained by granular media (soil).[68] So, changes in stiffness of those beads are accompanied by constrain-induced stresses. Highly transient phase transformations and constitutive changes occur in cheese-making during rennet-induced gelation process. Viscoelastic properties of cheese vary orders of magnitude during that process.[69] Since manufacturability-recently 3D-printability of cheese depends largely on mechanical properties, characterization in a non-destructive and real-time manner is essential in increasing yield and reducing food waste. In tissue engineering, tissue scaffolds made of biodegradable elastomers can experience almost 2.5-fold increase in modulus due to degradation, which may then alter the fate of the cells and resulting engineered tissue.[70] The non-destructive technique we demonstrated here can provide high throughput real-time characterization in all those applications. Through the current study we can observe that without internal stress formulation the errors to characterize the Young's modulus of evolving constrained soft materials can be large. As we illustrated in this work, vibration and wave-based techniques are promising candidates especially for *in operando* mechanical characterization of soft multiphasic materials.

Data availability

The data sets generated and supporting the findings of this article are obtainable from the corresponding author upon reasonable request. The authors attest that all data for this study are included in the paper.

Conflicts of interest

The authors declare that they have no known competing financial interests or personal relationships that could have appeared to influence the work reported in this paper.

Acknowledgements

This work is partially supported by the National Science Foundation (Grant no. CMMI-2200353 and CMMI-2224380) and the University of Wisconsin-Madison, Office of the Vice Chancellor for Research and Graduate Education with funding from the Wisconsin Alumni Research Foundation.

References

1 M. Doi, *J. Phys. Soc. Jpn.*, 2009, **78**, 052001.
2 J. L. Drury and D. J. Mooney, *Biomaterials*, 2003, **24**, 4337–4351.
3 B. Duan, L. A. Hockaday, K. H. Kang and J. T. Butcher, *J. Biomed. Mater. Res., Part A*, 2013, **101**, 1255–1264.
4 H.-W. Kang, S. J. Lee, I. K. Ko, C. Kengla, J. J. Yoo and A. Atala, *Nat. Biotechnol.*, 2016, **34**, 312–319.
5 D. Mohammadrezaei, N. Moghimi, S. Vandvajdi, G. Powathil, S. Hamis and M. Kohandel, *Sci. Rep.*, 2023, **13**, 1211.
6 E. Ozkaya, E. Triolo, F. Rezayaraghi, J. Abderezaei, W. Meinhold, K. Hong, A. Alipour, P. Kennedy, L. Fleysher, J. Ueda, P. Balchandani, M. Eriten, C. Johnson, Y. Yang and M. Kurt, *J. Mech. Behav. Biomed. Mater.*, 2021, **122**, 104680.
7 K. Yerrapragada, D. Chawla, C. Henak and M. Eriten, *Exp. Mech.*, 2023, **63**, 485–494.
8 J. Kim, L. Sapp and M. Sands, *Exp. Mech.*, 2022, **62**, 1615–1624.
9 M. N. I. Shiblee, K. Ahmed, M. Kawakami and H. Furukawa, *Adv. Mater. Technol.*, 2019, **4**, 1900071.
10 B. Wang, A. G. Moura, J. Chen, A. Erturk and Y. Hu, *Extreme Mech. Lett.*, 2020, **40**, 100841.
11 S. Schwarz, B. Hartmann, J. Sauer, R. Burgkart, S. Sudhop, D. Rixen and H. Clausen-Schaumann, *Exp. Mech.*, 2020, **60**, 1067–1078.
12 E. Sharon and E. Efrati, *Soft Matter*, 2010, **6**, 5693–5704.
13 F. Gao, C. Ruan and W. Liu, *Mater. Chem. Front.*, 2019, **3**, 1736–1746.
14 S. Taheri, G. Bao, Z. He, S. Mohammadi, H. Ravanbakhsh, L. Lessard, J. Li and L. Mongeau, *Adv. Sci.*, 2022, **9**, 2102627.
15 J. L. Drury, R. G. Dennis and D. J. Mooney, *Biomaterials*, 2004, **25**, 3187–3199.
16 J. A. Zimberlin, N. Sanabria-DeLong, G. N. Tew and A. J. Crosby, *Soft Matter*, 2007, **3**, 763–767.

17 S. Kundu and A. J. Crosby, *Soft Matter*, 2009, **5**, 3963–3968.
18 M. Czerner, L. A. Fasce, J. F. Martucci, R. Ruseckaite and P. M. Frontini, *Food Hydrocolloids*, 2016, **60**, 299–307.
19 A. Forte, F. Damico, M. Charalambides, D. Dini and J. Williams, *Food Hydrocolloids*, 2015, **46**, 180–190.
20 G. Han, C. Hess, M. Eriten and C. R. Henak, *J. Mech. Behav. Biomed. Mater.*, 2018, **84**, 28–34.
21 M. G. Espinosa, G. A. Otarola, J. C. Hu and K. A. Athanasiou, *J. R. Soc., Interface*, 2021, **18**, 20210765.
22 J. D. E. Dalisay, L. Liu, M. Eriten, L. A. Bergman and A. F. Vakakis, *Int. J. Solids Struct.*, 2022, **241**, 111482.
23 L. Liu, K. Yerrapragada, C. R. Henak and M. Eriten, *J. Vib. Acoust.*, 2022, **144**, 051003.
24 J. W. Hwang, D. Chawla, G. Han, M. Eriten and C. R. Henak, *J. Mech. Behav. Biomed. Mater.*, 2022, **126**, 105014.
25 G. Han, U. Boz, L. Liu, C. R. Henak and M. Eriten, *J. Vib. Acoust.*, 2020, **142**, 051113.
26 G. Han, U. Boz, M. Eriten and C. R. Henak, *J. Mech. Behav. Biomed. Mater.*, 2020, **110**, 103876.
27 R. Ramachandran and M. Nosonovsky, *Soft Matter*, 2014, **10**, 4633–4639.
28 C. Liu, B. Li, Z. Li, C. Cao, X. Gao, K. Zhang and H. Chen, *Soft Matter*, 2021, **17**, 6697–6706.
29 S. Malakooti, M. I. Hatamleh, R. Zhang, T. Taghvaee, M. Miller, Y. Ren, N. Xiang, D. Qian, C. Sotiriou-Leventis and N. Leventis, *et al.*, *Soft Matter*, 2021, **17**, 4496–4503.
30 C. Der Loughian, L. Tadrist, J.-M. Allain, J. Diener, B. Moulia and E. De Langre, *C. R. Mec.*, 2014, **342**, 1–7.
31 E. De Langre, O. Penalver, P. Hemon, J.-M. Frachisse, M.-B. Bogeat-Triboulot, B. Niez, E. Badel and B. Moulia, *Plant Phenomics*, 2019, 6379693.
32 M. Amabili, *J. Sound Vib.*, 2016, **362**, 142–156.
33 S. Le Guisquet and M. Amabili, *J. Mech. Phys. Solids*, 2023, **171**, 105152.
34 S. Schwarz, PhD thesis, Technische Universität München, 2021.
35 S. S. Yengul, P. E. Barbone and B. Madore, *Ultrasound Med. Biol.*, 2019, **45**, 586–604.
36 K. Arda, N. Ciledag, E. Aktas, B. K. Arbas and K. Köse, *Am. J. Roentgenol.*, 2011, **197**, 532–536.
37 C. Li, G. Guan, R. Reif, Z. Huang and R. K. Wang, *J. R. Soc., Interface*, 2012, **9**, 831–841.
38 C. Li, G. Guan, S. Li, Z. Huang and R. K. Wang, *J. Biomed. Opt.*, 2012, **17**, 057002.
39 A. Lucantonio, P. Nardinocchi and L. Teresi, *J. Mech. Phys. Solids*, 2013, **61**, 205–218.
40 Z. Li, Z. Liu, T. Y. Ng and P. Sharma, *Extreme Mech. Lett.*, 2020, **35**, 100617.
41 A. Pandey and D. P. Holmes, *Soft Matter*, 2013, **9**, 5524–5528.
42 D. P. Holmes, M. Roché, T. Sinha and H. A. Stone, *Soft Matter*, 2011, **7**, 5188–5193.
43 W. Howson and F. Williams, *J. Sound Vib.*, 1973, **26**, 503–515.
44 J. S. Jensen, D. Tcherniak and J. J. Thomsen, *J. Appl. Mech.*, 2000, **67**, 397–402.
45 K. Maes, J. Peeters, E. Reynders, G. Lombaert and G. De Roeck, *J. Sound Vib.*, 2013, **332**, 5417–5432.
46 L.-W. Chen and J.-L. Doong, *Int. J. Mech. Sci.*, 1984, **26**, 253–263.
47 A. Rosen and J. Singer, *J. Sound Vib.*, 1974, **34**, 357.
48 M. Amabili, P. Balasubramanian, I. D. Breslavsky, G. Ferrari, R. Garziera and K. Riabova, *J. Sound Vib.*, 2016, **385**, 81–92.
49 Y. Bai, B. Chen, F. Xiang, J. Zhou, H. Wang and Z. Suo, *Appl. Phys. Lett.*, 2014, 105.
50 P. G. d Gennes, *Scaling Concepts in Polymer Physics*, Cornell University Press, Ithaca, 1979.
51 S. Xu, Z. Zhou, Z. Liu and P. Sharma, *Sci. Adv.*, 2023, **9**, eade3240.
52 A. W. Leissa and M. S. Qatu, *Vibration of Continuous Systems*, McGraw-Hill, New York, 2011.
53 H. Deresiewicz and R. D. Mindlin, *J. Appl. Mech.*, 1955, **22**, 86–88.
54 M. Sachithanadam and S. C. Joshi, *J. Mater. Sci.*, 2014, **49**, 163–179.
55 M. Rossi, P. Nardinocchi and T. Wallmersperger, *Proc. R. Soc. A*, 2019, **475**, 20190174.
56 J. Yoon, S. Cai, Z. Suo and R. C. Hayward, *Soft Matter*, 2010, **6**, 6004–6012.
57 A. Lucantonio, P. Nardinocchi and L. Teresi, *J. Mech. Phys. Solids*, 2013, **61**, 205–218.
58 A. Pandey and D. P. Holmes, *Soft Matter*, 2013, **9**, 5524–5528.
59 S. Xu and Z. Liu, *J. Mech. Phys. Solids*, 2019, **127**, 94–110.
60 S. Chen, R. Huang and K. Ravi-Chandar, *Int. J. Solids Struct.*, 2020, **195**, 43–56.
61 J. D. Krehbiel, J. Lambros, J. A. Viator and N. R. Sottos, *Exp. Mech.*, 2010, **50**, 813–824.
62 R. E. D. Rudge, J. P. M. V. D. Sande, J. A. Dijksman and E. Scholten, *Soft Matter*, 2020, **16**, 3821–3831.
63 G.-Y. Li, Q. He, R. Mangan, G. Xu, C. Mo, J. Luo, M. Destrade and Y. Cao, *J. Mech. Phys. Solids*, 2017, **102**, 67–79.
64 Z. Abiza, M. Destrade and R. Ogden, *Wave Motion*, 2012, **49**, 364–374.
65 C. Ceccaldi, S. Strandman, E. Hui, E. Montagnon, C. Schmitt, A. Hadj Henni and S. Lerouge, *J. Biomed. Mater. Res., Part B*, 2017, **105**, 2565–2573.
66 R. Moucka, M. Sedlack and Z. Pátková, *Mech. Mater.*, 2023, **177**, 104559.
67 P. Zhu, R. Chen, C. Zhou, M. Aizenberg, J. Aizenberg and L. Wang, *Adv. Mater.*, 2021, **33**, 2008558.
68 J.-F. Louf, N. B. Lu, M. G. OConnell, H. J. Cho and S. S. Datta, *Sci. Adv.*, 2021, **7**, eabd2711.
69 R. Uribe-Alvarez, N. O'Shea, C. P. Murphy, C. Coleman-Vaughan and T. P. Guinee, *Food Hydrocolloids*, 2021, **114**, 106542.
70 K. Kim, C. G. Jeong and S. J. Hollister, *Acta Biomater.*, 2008, **4**, 783–790.

